Analysis of equatorial x-ray diffraction patterns from skeletal muscle

Leepo C. Yu

National Institutes of Health, Bethesda, Maryland 20892

ABSTRACT Some of the factors that affect the intensities and the phases of the first five equatorial x-ray reflections from skeletal muscle are studied by simplified models describing axially projected mass distributions in unit cells. Examples of mass distributions that produce various phase combinations and intensities are presented. Effects due to radial movement of crossbridges and those due to mass transfer between the thick filament and the thin filament regions are compared. In addition, the study suggests that some features in the reconstructed filament structures could be due to the consequences of limited resolution.

INTRODUCTION

X-ray diffraction has been instrumental in providing structural information on muscle cells. The hexagonal lattice formed by the interdigitating thick and thin filaments gives rise to a series of reflections on the equator. Such equatorial diffraction patterns contain information about the mass distribution projected axially onto a plane perpendicular to the fiber axis. Most frequently, the two prominent reflections, [1, 0] and [1, 1], are recorded. The two-dimensional electron density maps reconstructed from these two reflections provide structural information at 280 Å spatial resolution. Mass transfers between the two regions of filaments can be calculated, but with very little detailed information as to which part of the filament is affected. Additional reflections have been recorded from the frog sartorius muscle (Huxley and Brown, 1967; Yu et al., 1977); from single, chemically-skinned rabbit psoas fibers (Yu and Brenner, 1986, 1989) and from the intact fin muscle of plaice fish (Harford and Squire, 1986). With five reflections ([1, 0], [1, 1], [2, 0], [2, 1], [3, 0]) from the sartorius and seven reflections ([2, 2] and [3, 1] in addition) from the psoas muscle and the plaice fish, the spatial resolution improves to 130 and 100 Å, respectively. Electron density maps reconstructed from the additional reflections reveal new features. In particular, it is possible to resolve the distribution of the myosin heads from the thick filament backbone (Yu et al., 1985; Yu and Brenner, 1989).

However, reconstruction of the density maps of muscle cells is handicapped by the lack of phase information and the small number of reflections recorded experimentally. Because the standard crystallographic methods are not yet applicable to muscle, phase information cannot be determined experimentally by x-ray diffraction. Yet, phase assignment has distinct effects on the apparent features of the reconstructed density maps. As shown in our earlier work (Yu et al., 1985), the apparent structures in the density maps of muscle cells derived from five equatorial reflections were altered significantly by changing one single phase. The second complicating factor in reconstructing density maps is the problem associated with series termination. Theoretically, an infinite number of reflections with correct phases is required to completely reconstruct the original structure. If the Fourier series is terminated after a small number of terms, i.e., if the number of reflections is limited, artifacts might be created. The possibility of artifacts complicates the interpretation of reconstructed density maps and hence the selection of phases. For instance, a phase combination that produces a density map containing very low density level at the thin filament location ought to be rejected, if this feature is not a result of series termination. One approach to reduce ambiguities is to model mass distributions in the unit cells and calculate the Fourier transforms. From the resulting phases and intensities, one could then derive an estimate as to what are the likely density distributions that are consistent with the experimental data, aiding the process of phase selection.

The purpose of the present modelling study is twofold: first, to improve understanding of the factors that affect the phases and the intensities of the equatorial diffraction patterns from skeletal muscle; second, to examine the effects of series termination on reconstructed density maps. For the first purpose, Fourier transforms, hence the intensities and the phase angles, are calculated based on a wide variety of density distributions which approximately resemble the known basic structures of skeletal muscle cells. Thus, variations in the phases, as a function of density distributions, can be followed systematically. For the second purpose, series termination is accomplished by first calculating the Fourier transforms based on given

density distributions, and subsequently eliminating the higher order terms in the reciprocal space. The reconstructed density distributions based on the limited number of terms are compared with the original distributions, thereby effects of the series termination are examined.

A brief account of the work has appeared previously (Yu, 1987).

METHODS

The basic features of the models are shown in Fig. 1. Independent parameters are assumed for the backbone of the thick filament and the surrounding distribution of myosin heads. Similar assumptions are made for the thin filament and the attached crossbridges. Myosin heads in axial projection are assumed to be distributed in a continuum. The center to center distance between the thick filaments (the lattice constant) is assumed to be 44 nm.

To model the densities of various elements, such as the thick filament backbone, it is necessary to assume particular functional forms for the distributions. Several different sets of functions have been used. Those chosen are: (a) all distributions are Gaussian functions:

$$G_i(r) = \frac{A_i}{2\pi\sigma_i^2} \exp\left(-r^2/2\sigma_i^2\right)$$

$$\text{for } i = M, A$$
$$M = \text{thick filament backbone}$$
$$A = \text{thin filament} \qquad (1)$$

$$G_i(r) = \frac{A_i}{2\pi\sigma_i^2} \exp\left[-(r - R_i)^2/2\sigma_i^2\right]$$

$$\text{for } i = H, B$$
$$H = \text{myosin heads}$$
$$B = \text{attached crossbridges,} \qquad (2)$$

where i stands for each region of M, A, H, and B and r is the distance from the center of M or A. A_i and σ_i are parameters for the amplitudes and standard deviations. R_i, $i = H$, B, are the radial distances of the centers of the annular rings of mass (myosin heads [H] and the attached crossbridges [B]), surrounding the backbone and the thin filament, respectively.

In Eqs. 1 and 2, A_i, i.e., A_M, A_A, A_H, and A_B, are defined as the masses of M, A, H, and B, respectively. In each unit cell the total mass is equal to $(A_M + 2A_A + A_H + 2A_B)$. The diameters of the filaments in Eq. 1 are defined to be equal to $4\sigma_M$ and $4\sigma_A$, respectively.

(b) Gaussian functions for the backbone of the thick filament (M) and the thin filament (A) but the distributions for the myosin heads (H) and the attached crossbridges (B) are flat functions, i.e., Eq. 2 is replaced by

$$F_i(r) = \rho_i \quad \text{for } i = H, B \quad \text{and} \quad R_i - w_i \le r \le R_i + w_i, \qquad (3)$$

where ρ_i are the constant density levels and w_i are the half widths of the annular rings.

(c) All distributions consist of flat topped functions at the centers with cosine shaped edges.

$$C_i(r) = \rho_i \quad \text{for } i = M, A \quad \text{and} \quad 0 \le r \le R_i$$
$$= \rho_i/2\{1 + \cos\left[\pi(r - R_i)/E_i\right]\}$$
$$\text{for} \quad R_i \le r \le R_i + E_i, \qquad (4)$$
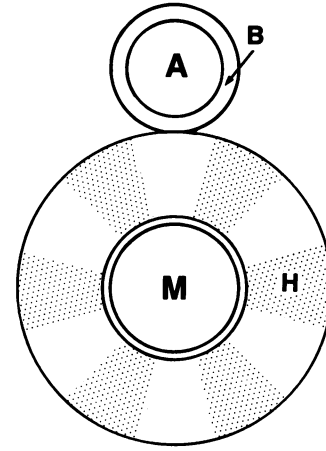
where $\rho_i = A_i/\{\pi R_i^2 + \pi E_i [E_i/2 + R_i - 2E_i/\pi^2]\}$, R_i and E_i are radii of the cores and the sizes of the edges, respectively. Furthermore,

$$C_i(r) = \rho_i \quad \text{for } i = H, B \quad R_i - w_i \le r \le R_i + w_i$$
$$= \rho_i/2(1 + \cos\{\pi[(r - R_i - w_i)/E_i]\})$$
$$R_i + w_i \le r \le R_i + w_i + E_i$$
$$= \rho_i/2(1 + \cos\{\pi[(r - R_i + w_i)/E_i]\})$$
$$R_i - w_i - E_i \le r \le R_i - w_i, \qquad (5)$$

where $\rho_i = A_i/\{4\pi R_i w_i + \pi E_i[E_i + 2 R_i]\}$.

This type of function covers a broad range of distributions and requires a large number of parameters, and hence is the most flexible.

The distribution H surrounding the backbone of the thick filament needs not be uniform. In fact, to match experimental intensity data, the distribution is often assumed to be nonuniform. To simplify calculations, the nonuniformity assumes a sixfold symmetry, as described in Fig. 1. The parameter RATIO defines the nonuniformity:

$$\rho_H(\text{high}) = \rho_H(\text{average}) * \text{RATIO} \qquad (6)$$

$$\rho_H(\text{low}) = \rho_H(\text{average}) * (2 - \text{RATIO}), \qquad (7)$$

where RATIO ranges between 1 and 1.5. The region directly between M and A is the high density region, $\rho_H(\text{high})$, as the unshaded region shown in Fig. 1.

Effects of series termination were modeled by first performing Fourier transforms on the functions assumed to be the original density distributions. In the reciprocal space, a smooth varying digital filter with a sharp cut-off was imposed on the transformed functions so that only a specified number of terms remained. For example, if only five orders were to remain, the filter leaves the intensities of the first five orders unchanged, but the reflections of higher orders were set to be zero. This manipulation closely simulated the empirical way of reconstructing electron density maps (Yu et al., 1985; Yu and Brenner, 1989), since reconstruction was limited to five or seven reflections only. The exact form of the filter is illustrated in Fig. 2. Other filters such as Gaussian filters were found to be inappropriate, since any function with a significant "tail" extending beyond the five or seven reflections only modulates but does not exclude the higher order amplitudes, and hence the Fourier series are not terminated in the same manner as the experimental observations. After filtering in the reciprocal space, inverse Fourier transform resulted in two-dimensional density maps which were then compared with the original input structures to obtain the effects of series termination.

The calculations and subsequent display of density maps were carried out by using the PIC system (Trus and Steven, 1981) on a VAX 11/780. The hexagonal lattice is represented as pseudorectangular lattice with one thick filament at the center of the lattice (Fig. 3). Photographic copies of the density maps were recorded by a camera station (Matrix, Inc., Mesa, AZ).

RESULTS

Series of models with a wide range of parameters were calculated to obtain the corresponding equatorial diffraction intensities and phases. Since there is great interdependence among the parameters in determining the results, a definitive cause and effect relationship between a parameter and one particular reflection can only be
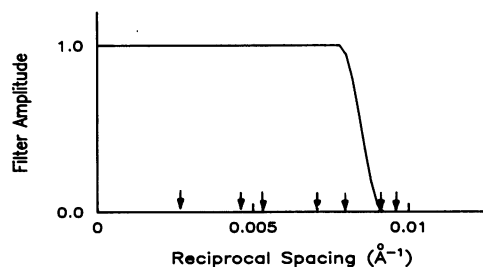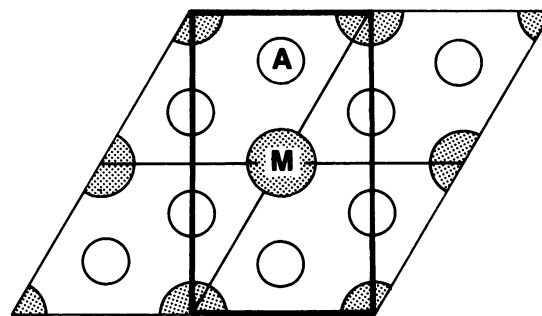
FIGURE 3 The psuedo-rectangular lattice representation, shown in bold outline, of the hexagonal myofilament lattice which was used in performing Fourier synthesis using the PIC system (Trus and Steven, 1983). M, thick filament; A, thin filament. All the models assume that the lattice spacing between the [1, 0] planes, d_{10}, is 38 nm. The surface to surface distance between M and A is approximately 10 mm, depending on the diameters of the filaments.

stated qualitatively. The results indicate that in general, phases are very sensitive to the spatial characteristics of the density distributions in the unit cell, while the magnitude of density levels tends to modulate the intensities. However, because the models are assumed to be centrosymmetric, a phase change takes place when an intensity crosses the zero level. Typical distributions used in modeling are shown in Figs. 4 and 5. The functions describing the distributions in Fig 4 a are of the type c (flat functions, see Eqs. 4 and 5) described earlier. The results shown below, however, are qualitatively insensitive to the type of functions used.

Effects of density distributions on the equatorial phases

As expected, density distributions in unit cell have profound effects on the resultant phases of the equatorial diffraction patterns. Examples of the relations between unit cell structures and the corresponding first five equatorial phases, i.e., the phases of [1, 0], [1, 1], [2, 0], [2, 1], and [3, 0], are illustrated in Fig. 6, where density profiles along the lines drawn through the centers of A-M-A are shown. Some general qualitative conclusions can be stated: (a) a 180° phase of [3, 0], ϕ_{30}, is associated either with a low density thin filament A or a low density thick filament backbone M (Fig. 6, a–c); (b) a 180° ϕ_{21} is frequently associated with a low density core at the center of the backbone M (Fig. 6, b, c, e; the exception being g); (c) a 0° ϕ_{21}, on the other hand, indicates the peak density of the unit cell being located at the center of the backbone M. Moreover, the combination (+ + + + +) (Fig. 6 d) requires a very high density of M compared with the distribution H or the thin filament A. The combination

FIGURE 2 A radial filter used in reciprocal space to model the effect of series termination. The filter has the value of unity up to 0.0078(Å^{-1}) ([3, 0] in real space) and then falls off to zero at 0.0093(Å^{-1}) (between [2, 2] and [3, 1]) along the path of the form $\{1 + \cos[\pi(x - 0.0078)/0.0015]\}/2$ with $0.0078 \leq x \leq 0.0093$. The application of this filter is referred to in the text as cutoff at [3, 0]. In practice, the calculated Fourier amplitudes of the models are multiplied by the filter function in the reciprocal space. The arrows indicate the reciprocal spacings of the Bragg planes [1, 0], [1, 1], [2, 0], [2, 1], [3, 0], [2, 2], and [3, 1]. By applying this filter, the amplitudes of the first five reflections are multiplied by unity, whereas reflections beyond [2, 2] are reduced to zero. Other filters used include cutoff at [1, 1] and at 0.025 Å^{-1}.
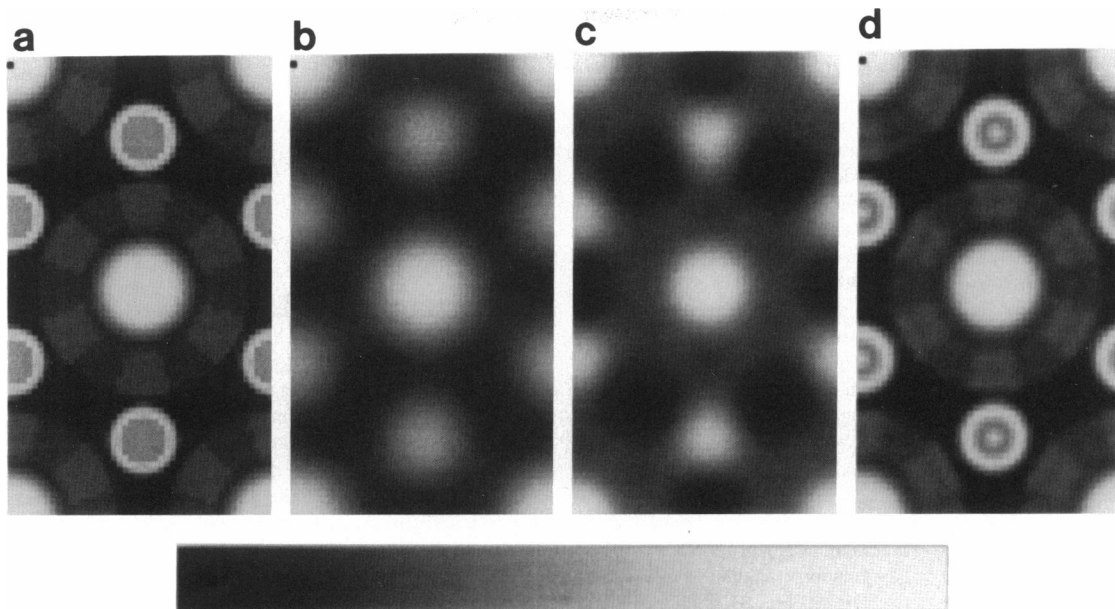
FIGURE 4 Density maps showing the effect of series termination. On the gray scale, the lightest tone represents the highest density. (*a*) A model using flat + cosine functions as defined in Eqs. 4 and 5 with parameters (see text for definitions) in arbitrary units $A_m = 52$, $A_A = 16$, $A_H = 58$, $A_B = 8$, and in nm: $w_M = 11$, $w_A = 7$, $w_H = 5$, $w_B = 1.5$; $E_M = 4$, $E_A = 4$, $E_H = 3$, $E_B = 0.5$; $R_H = 14$, $R_B = 5$, and RATIO $= 1.2$. (*b*) The density map reconstructed with cutoff at [1, 1]. (*c*) The density map reconstructed with cutoff at [3, 0]. (*d*) The density map reconstructed with cutoff at 0.025 $Å^{-1}$ in the reciprocal space.

$+ + + - +$ for the first five reflections shows a distribution of H located very close to the backbone ($R_H \sim 8$–10 nm) (Fig. 6 *e*). Combining the two densities, H and M, in their overlapping area near the edge of M creates a dip in density at the center of the M. $(+ + - + +)$ consistently requires a high density core at the center of M and the center of the distribution H located at ~13–15 nm from the center of the backbone (Fig. 6, *f*, *g*). A phase combination of $(+ + - - +)$, on the other hand, is either consistent with a low density core at the backbone M, similar to Fig. 6 *e* ($R_H \sim 8$–12 nm), or with no or very little overlap between the distribution of H and the thin filament A (Fig. 6, *g*).

Effects of the location of myosin heads on intensities and phases

Because the mass ratio of the thick filament backbone M, the thin filament A, and myosin heads H is constrained by the biochemical data, the parameters of interest mainly lie with the radial position and width of the annular distribution of H. As it is shown in Fig. 6, the distribution H has a profound effect on the phases of [2, 0], [2, 1], and [3, 0]. Table 1 shows the effects in more detail, with the mass ratio assigned in the range consistent with biochemical data. Table 1 shows that as the radial position, R_H, of the center of myosin heads H extends towards the thin

filament A, phase of [3, 0] changes from 180° to 0° and I_{30} increases. Effects of R_H are not limited to [3, 0]. An increase in R_H produces changes in the intensities and the phases of almost all the reflections studied. In particular, a decrease of a factor of 15 in I_{10} is calculated as R_H increases from 8 to 16 nm. As R_H is increased, the phases and the intensities of [2, 0] and [2, 1] change accordingly, crossing zero at ~9 nm and again at 15 nm, and at 13 nm, respectively. The notable exception here is [1, 1], which remains almost unchanged if R_H is $\gtrsim 10$ nm. Meanwhile, the phases of [2, 2] and [3, 1] change through three combinations as R_H is increased.

Effects of parameters other than R_H were also studied. For instance, variations in the width of the distribution H do not change the phases as readily as shown in Table 1. Increasing mass of myosin heads A_H, prominently increases I_{20} (e.g., increasing A_H by ~33% and keeping all other parameters constants lead to an increase in I_{20} by ~100%). Increasing the parameter RATIO (i.e., increasing mass in the unshaded area vs. the shaded area [Fig. 1] while the total mass of myosin heads, A_H, remains constant) decreases I_{30}, but increases [2, 0], [2, 1], and [3, 1] while [1, 0] and [1, 1] are not affected. For instance, if RATIO in Table 1 at $R_H = 14$ nm were changed from 1.0 to 1.2, the intensities now read 2,061, 3,771, 41, 247, 350, 62, and 0 in the same order as listed in Table 1.
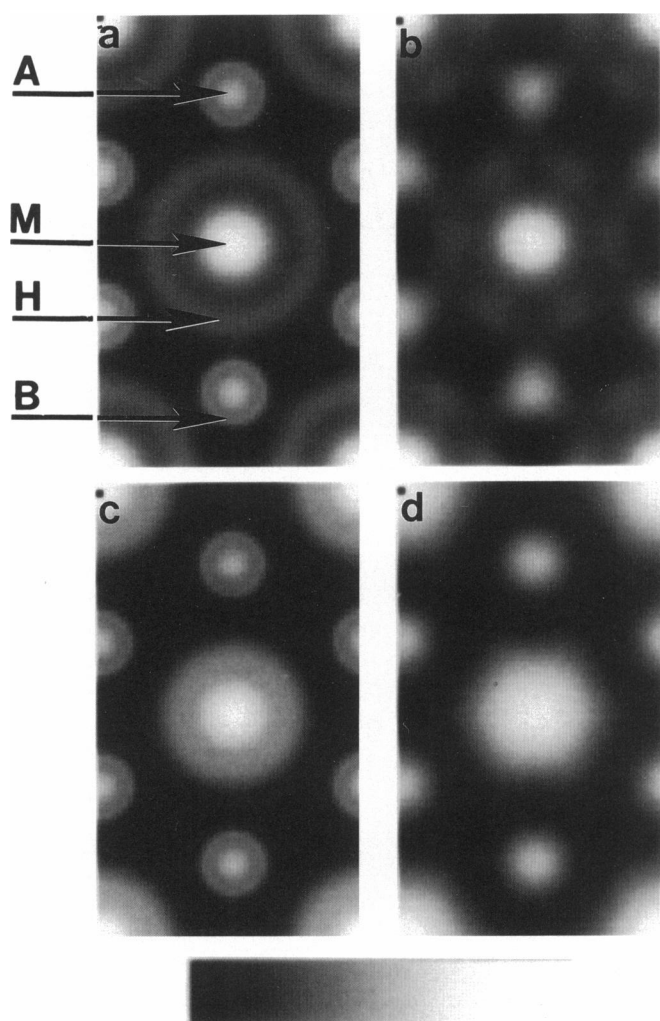
FIGURE 5 Spurious details are created by series termination, with cutoff at [3, 0]. (*a* and *c*) Gaussian function models, with $A_M = 52$, $A_A = 16$, $A_H = 56$, $A_B = 5$, and in nm: $\sigma_M = 4.5$, $\sigma_A = 3.5$, $\sigma_H = 2.5$, $\sigma_B = 0.75$, $R_B = 4$. (*Top*) $R_H = 13.5$ nm; (*bottom*) $R_H = 10$ nm. (*b* and *d*) Reconstructed density maps with reflections cut-off at [3, 0] by using the same filter as shown in Fig. 2.

refleciton intensities. Table 1 illustrates the sensitivity of intensities and phases of the reflections due to radial movement. In contrast, mass transfer from the annular region H to the region B has been shown to affect the intensities I_{10} and I_{11} in a reciprocal way, i.e., I_{10} decreases and I_{11} increases by approximately the same amount (Huxley, 1968; Lymn, 1978). Our calculations as shown in Table 2 agree, although the magnitude of decrease in I_{10} is somewhat less than the increase in I_{11}. Table 2 further shows that all of the higher order reflections up to [3, 1] decrease to some extent. All the phases remain unchanged. The distinctly different characteristic changes in the reflection intensities could be used to distinguish the two types of mass movement.

Effects of series termination

The second part of this study is to determine the effects of series termination. Sample distributions such as Figs. 4 and 5 are used to demonstrate such effects. Fig. 4. where the mass in the annular region H is assumed to have sixfold symmetry, shows that the reconstructed density maps begin to resemble the original one (Fig. 4 *a*) if the number of terms (i.e., reflections) used in reconstruction reaches approximately the tenth order of [1, 0] at spatial resolution of 40 Å (Fig. 4 *d*). With less number of reflections, some features are exaggerated, while others smeared.

Cutoff at [1, 1] reflection

If reflections beyond [1, 1] were set to zero by the radial filter (Fig. 2), the mass distribution in the reconstructed density map shows that the region H is smeared out and the peak density of the thin filament is greatly reduced (Fig. 4 *b*). Density maps reconstructed on the basis of experimental [1, 0] and [1, 1] intensities typically show these two characteristics.

Distinct effects on reflection intensities of radial movement and mass transfer of crossbridges

"Radial movement" and "mass transfer" of crossbridges involve two different types of mass movement: in radial movement the distribution of myosin heads remains centered around the thick filament lattice points, while the center of mass moves away from the center of the backbone; whereas mass transfer removes mass from the region H surrounding the thick filament backbone to the region B centered around the thin filament. The two types of movement have distinctly different effects on the

Nonuniformity and spurious symmetry may be created in the reconstructed density maps

We found that exaggerated sixfold symmetry is frequently created in the annular region H, if the original distribution is uniform. Fig. 5 shows that series termination at five or seven reflections ($\sim\frac{1}{100}$ Å^{-1}) creates strong sixfold symmetry that is absent from the original distribution. The creation of this apparent extra structure is somewhat insensitive to the radial location of the halo of mass. In Fig. 5, the radial positions of the center of the region H are 10 nm (Fig. 5 *a*) and 13.5 nm (Fig. 5 *c*), respectively.
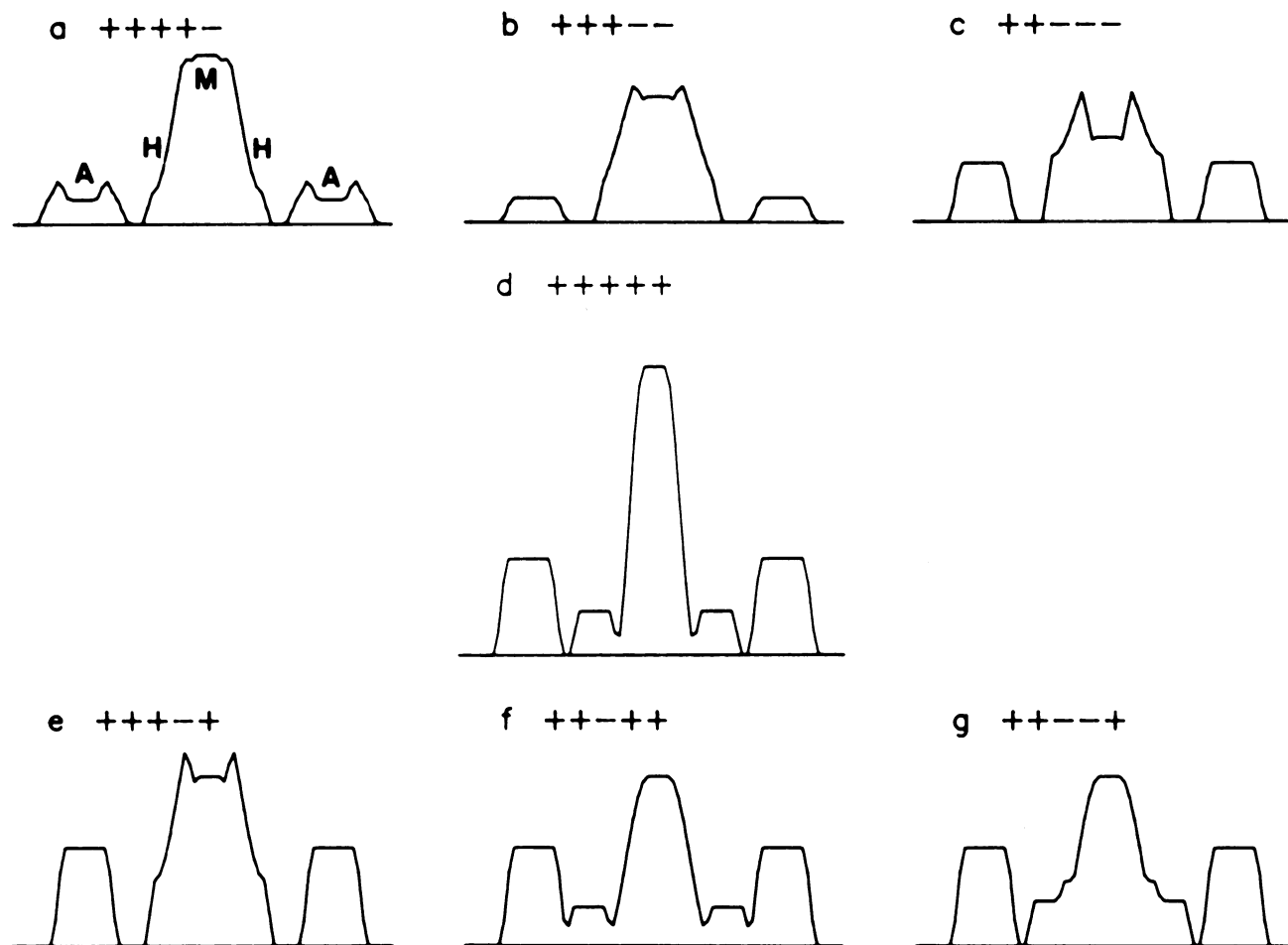
FIGURE 6 Examples of density distributions and their corresponding first five equatorial phases[f]; General Characteristics of Density Profiles[*]; (a) Density of A very low, particularly at the center; H is located close to the center of M, and fused into the surface boundary of M. (b) Density of A very low; H fused into the backbone at M. (c) The prominent H and the low density of the backbone M create an apparently semi-hollow structure; peak density of A comparable to peak density of M (both low). (d) Density at the center of M highest in the unit cell; density of M very high compared to H and A; diameter of M, narrow; H extended away from M. (e) H located close to center of M (~8 nm), fused into the surface of M, creating a dip in density at center of M. (f) Highest density in the unit cell located at the center of M; H located at ~13nm from center of M; H not overlapping significantly with backbone M. (g) Center of annulus H ≤ 12 nm from center of M; distribution of H does not overlap significantly with A.

*Density profiles are drawn along the line passing through the centers of A-M-A.

[f]The distributions shown in (a)–(g) are of the flat + cosine function type (Eq. 4–5). Density levels are given in uniform but arbitrary units. A represents thin filament; H, myosin heads; M, thick filament backbone.

Nonuniform distribution
may appear uniform

If the reflections are cutoff at [3, 0] (~$\frac{1}{130}$ Å^{-1}), the distribution of H is resolved from the thick filament backbone (Fig. 4 c). However, we assumed two density levels in the region H (Fig. 4 a) with the higher density level situated directly between the thin and the thick filaments. The ratio of these two levels, defined by the parameter RATIO, is 1.2. After the truncation, the originally nonuniform distribution now appears relatively uniform. In fact, the density level directly between M and A appears to be slightly lower relative to the neighboring region. To achieve the same effect (i.e., nonuniform → uniform), the magnitude of RATIO can vary somewhat, depending on the functions used to describe the density distributions. For example, if the Gaussian functions were used instead of flat + cosine functions, to achieve similarly uniform distribution as in Fig. 5 c, RATIO needed is 1.4.

Improvement of accuracy in reconstruction depends on the original distribution. Clearly, the weaker the higher order reflections are, the less effect would be caused by series termination. For example, if the filaments are far apart, or the H region is located very close to the thick

R_H	Phases‡	I_{10}	I_{11}	I_{20}	I_{21}	I_{30}	I_{22}	I_{31}
8	+++−+−−	10,465	7,639	0	419	0	0	0
9	++−−++−	8,718	6,190	0	436	0	0	0
10	++−−+++	7,041	5,070	70	282	141	0	0
11	++−−+++	5,506	4,240	110	110	220	55	55
12	++−−+++	4,146	3,773	124	0	373	83	41
13	++−++++	2,995	3,594	60	30	509	60	0
14	++−+++−	2,059	3,665	20	165	556	21	0
15	++++++−	1,334	3,987	0	293	494	0	27
16	+++++−−	804	4,559	72	330	370	0	56

A_H‡	A_B	Phases	I_{10}	I_{11}	I_{20}	I_{21}	I_{30}	I_{22}	I_{31}
64	0	++−+++−	3,439	2,050	3	248	626	62	14
62	1	++−+++−	3,239	2,280	3	230	609	55	13
60	2	++−+++−	3,045	2,521	3	213	588	49	9
58	3	++−+++−	2,857	2,777	3	197	568	40	8
56	4	++−+++−	2,675	3,047	3	179	551	35	8
54	5	++−+++−	2,499	3,326	2	165	532	30	5
52	6	++−+++−	2,329	3,619	2	149	515	23	5

filament, the reflections beyond [3, 0] are rather insignificant (Table 1). Hence, few reflections are needed to arrive at a density map reasonably similar to the original one. In fact, effects of cutoff at [3, 0] are minimal if there is no extra mass between the backbone of the thick filament and the thin filament as was found earlier (Yu et al., 1985). If, on the other hand, the H distribution fills the interfilament space, discrepancies between the original and the reconstructed distributions persist until the resolution is improved to well below 100 Å, as it is demonstrated in Fig. 4, b–d. In such cases, intensities beyond [3, 0] are significant.

DISCUSSION

Equatorial x-ray diffraction provides structural information about the myofilaments in their native state. However, the technique is limited by the lack of phase information and the noncrystalline nature of the filament packing. For these reasons, interpretation of the reconstructed density maps is not straightforward. The present study suggests that some of the features in the reconstructed density maps obtained experimentally could be a consequence of limited resolution. It is shown that series termination could produce an enlarged and triangle-shaped thin filament even though the original distribution is circularly symmetric (Figs. 4 a and c; 5, a and b). A uniformly distributed mass surrounding the backbone could become nonuniform in the reconstructed maps (Fig. 5), and vice versa (Fig. 4, a, b, and c). The magnitude of the series termination effect, however, depends on the original mass distribution. If the higher order reflections are weak, the cut-off effect would not be prominent.

If there were no reflections beyond the cut-off, obviously, the reconstructed density maps faithfully represent the original distributions (if the phases are known). However, the examples illustrated in the present study should serve as a precautionary note in interpreting the reconstructed density maps.

Because of the possibility of artifacts present in the reconstructed density maps, the present modeling approach is useful in extracting information from such maps. As a result of the modeling, it is possible to estimate, albeit approximately, the underlying mass distributions without spurious features that produce various combinations of phases and intensities.

Lymn (1978) showed that both the number of cross-bridges attached to the thin filament and the configuration of the attachment could affect the intensities of [1, 0] and [1, 1]. The present calculations deal with the axially projected mass distributions. The calculations include the thick filament backbone and the intensities of the higher order reflections are studied in addition to [1, 0] and [1, 1]. The calculations suggest that in a unit cell with the lattice constatnt being 44 nm, a phase combination of (+ + − + +) signifies that the center of mass of myosin heads is probably located at ~13–15 nm from the center of the backbone, while (+ + − − +) is at ~11–12 nm and (+ + + − +) is at ~8–10 nm (Table 1). Without the calculations, it is difficult to derive such information directly from the reconstructed density maps, since the myosin head distribution is generally masked by the limited resolution smearing and the spurious sixfold symmetry. Moreover, calculations indicate that a 180° phase of [3, 0] very likely originates from either a very low density level at the center of the thin filament or a semi-hollow structure of the thick filament, which is incompatible with currently known structural data of the filaments. A 180° phase of [2, 1] and [1, 2], on the other hand, appears to signify that the myosin heads are packed

closely to the backbone and there is little overlap between myosin head distribution and the thin filament.

One of the implications of the present results is that phases and intensities of the equatorial reflections are likely to depend on the experimental conditions the muscle is subjected to. For example, if under one condition, the myosin heads are somehow compressed or brought to retract against the thick filament backbone, the phases for the first five reflections could be $(+ + + - +)$ or $(+ + - - +)$; if under another condition where the myosin heads are distributed between the filaments, the phases could be $(+ + - + +)$. However, whether a change of phase takes place could be determined by following the variations in the intensities, which should cross the zero level, as the experimental conditions are changed in a graded way.

The modeling also points to the importance of studying individual reflections instead of intensity ratios. The information of the two types of mass movement as illustrated in Tables 1 and 2 would be lost if only the intensity ratio I_{11}/I_{10} were studied. Normalization procedures other than using I_{10} from each diffraction pattern (see for example, Yu and Brenner, 1989) provide additional information on structural changes in the unit cell.

SUMMARY

In the present study, some typical mass distributions that produce various combinations of phases and intensities of the equatorial diffraction are illustrated. Modeling suggests that the first seven reflections, with the exception of [1, 1], are very sensitive to the radial position of the center of mass of the density distribution of myosin heads surrounding the backbone of the thick filament. This is in sharp contrast to those changes brought by mass transfer from thick filament region to center around the thin filament.

Limited resolution could introduce extra details or exaggerated symmetry to the reconstructed distributions in the unit cell. The degree of prominence of the spurious details depends on the original distribution and the number of reflections included in the Fourier synthesis. Given these limitations, modelling is essential in interpreting density maps reconstructed from equatorial x-ray diffraction data.

REFERENCES

Harford, J., and J. Squire, 1986. "Crystalline" myosin crossbridge array in relaxed bony fish muscle. *Biophys. J.* 50:145–155.

Huxley, H. E., and W. Brown, 1967. The low-angle X-ray diagram of vertebrate striated muscle and its behavior during contraction and rigor. *J. Mol. Biol.* 30:383–434.

Huxley, H. E. 1968. Structural difference between resting and rigor muscle: evidence from intensity changes in the low angle equatorial X-ray diagram. *J. Mol. Biol.* 37:507–520.

Lymn, R. W. 1978. Myosin sub-fragment-1 attachment to actin: expected effect on equatorial reflections. *Biophys. J.* 21:93–98.

Trus, B. L., and A. C. Steven, 1981. Digital image processing of electron micrographs: the PIC system. *Ultramicroscopy.* 6:383–386.

Yu, L. C., R. W. Lymn, and R. J. Podolsky, 1977. Characterization of a non-indexible equatorial X-ray reflection from frog Sartorius muscle. *J. Mol. Biol.* 115:455–464.

Yu, L. C., A. C. Steven, G. R. S. Naylor, R. C. Gamble, and R. J. Podolsky, 1985. Distribution of mass in relaxed frog skeletal muscle and its redistribution upon activation. *Biophys. J.* 47:311–321.

Yu, L. C., and B. Brenner, 1986. High resolution equatorial x-ray diffraction from single skinned rabbit psoas fibers. *Biophys. J.* 49:133–135.

Yu, L. C. 1987. Effects of limited resolution on density maps reconstructed from equatorial x-ray diffraction intensities of skeletal muscle. *Biophys. J.* 51(2, Pt. 2):473a. (Abstr.)

Yu, L. C. and B. Brenner. 1989. Structures of actomyosin crossbridges in relaxed and rigor muscle fibers. *Biophys. J.* 55:441–453.